Numerical model and parametric analysis of a liquid based hybrid photovoltaic-thermal (PVT) collector

Madalina Barbu, Monica Siroux, George Darie

Energy Reports 7 (2021) 7977–7988

Contents lists available at ScienceDirect

Energy Reports

journal homepage: www.elsevier.com/locate/egyr

Numerical model and parametric analysis of a liquid based hybrid photovoltaic thermal (PVT) collector

Madalina Barbu [a,b], Monica Siroux [b,*], George Darie [a]

[a] Department of Energy Generation and Use, Faculty of Power Engineering, University POLITEHNICA of Bucharest, Bucharest, Romania
[b] INSA Strasbourg ICUBE, University of Strasbourg, Strasbourg, France

ARTICLE INFO

Article history:
Received 18 December 2020
Received in revised form 24 June 2021
Accepted 19 July 2021
Available online 4 August 2021

Keywords:
Renewable energy
Solar energy
PVT
Micro-cogeneration
Heat transfer
Dynamic simulation

ABSTRACT

A hybrid photovoltaic thermal (PVT) panel is a module in which the photovoltaic (PV) layer is not only producing electricity, but also operates as a thermal absorber. As a result, thermal and electrical energy are being produced simultaneously, operating as a micro-cogeneration equipment. As in any cogeneration system, there is tight link between the electrical and thermal performance and it is dependent on multiple parameters: climate conditions, thermo-physical, geometrical and electrical properties. This paper investigates the effect of the variation of several of these parameters on the electrical and thermal performance, as well as on the global output. In order to achieve this, a dynamic numerical model is proposed, which simulates the heat exchange between the layers of the PVT panel. The model was applied to two different climatic conditions: Bucharest, Romania and Strasbourg, France, in order to assess and compare their behavior and performance. The simulation computes the temperature of each layer at any particular time, and a slightly higher outlet temperature of the working fluid can be observed in Bucharest during the summer, and in Strasbourg during the winter. The model is validated against data from the literature and can be applied to any climatic conditions and adapted for multiple geometrical and thermo-physical configuration. Next, a one-factor-at-a-time parametric analysis is carried out in order to assess the impact of various parameters on the electrical, thermal and global efficiency. The results showed in most cases a compromise between the electrical and thermal performance: in terms of wind speed and insulation, the thermal benefits of low wind and high insulation overcome the decrease in electrical efficiency. The packing factor was found to be optimum when maximized, as the electrical benefits are more significant than the thermal loss. The width of the channels in the heat exchanger should also be maximized as far as technologically possible for best performance.

1. Introduction

Solar energy is among the most promising renewable sources, playing an essential role in the energy mix of the future. Energy can be extracted from the sun in the form of heat or electricity, by means of the established solar technologies currently available on the market: solar thermal (ST) panels and photovoltaic panels (PV). Several comprehensive reviews on the latest solar technologies has been carried out (Ahmadi et al., 2018; Khatibi et al., 2019) comparing and contrasting some of the technologies in terms of economic feasibility and CO_2 emissions.

Hybrid photovoltaic–thermal (PVT) collectors combine and maximize the benefits of these two types of energy extraction technologies into one single equipment, and can produce simultaneously electrical and thermal energy. This allows for a higher overall conversion efficiency of the incident solar radiation compared to individual PV or ST panels.

PVT collectors are a type of micro-cogeneration technology that can be very efficiently integrated into domestic households and can achieve decentralized production of clean heat and energy for the end consumer. Furthermore, PVT systems can obtain an overall better payback of the initial investment compared to individual side-by-side PV and ST panels (Ramos et al., 2017; Barbu et al., 2019c). Along with the financial benefits, PVT systems have several additional advantages. Firstly, by extracting the heat losses that occur during the photovoltaic conversion through the processes of thermalization and non-absorption, the overall system efficiency increases. Also, the electrical efficiency of the constituent PV cells is improved as a result of a lower operating temperature. Normally, the PV cells decrease in efficiency when operating in high temperatures. Most of them lose about 0.3–0.9% for each °C above their standard operating temperature of 25 °C (Dubey et al., 2013). Thus, by cooling the cells through the

* Corresponding author.
E-mail addresses: madalina.manole0401@upb.ro (M. Barbu), monica.siroux@insa-strasbourg.fr (M. Siroux), geo@energy.pub.ro (G. Darie).

https://doi.org/10.1016/j.egyr.2021.07.058

heat collector, the PV cells in PVT systems can have a 4%–12% better performance compared to the stand-alone PV module (Ramos et al., 2017). By combining the electrical and thermal components, the global efficiency of the system is improved, since the global efficiency η_{GL} can be written the sum between the electrical efficiency η_{EL} and the thermal efficiency η_{TH}.

This solution is particularly interesting and cost-efficient for small scale applications, where heat and electricity are required simultaneously, and roof and facade space are limited, especially in urban locations. In addition, several studies (Barbu et al., 2019c; Herrando and Markides, 2016) investigate the economic benefits of the PVT systems compared to individual side-by-side PV and solar-thermal panels, showing that the PVT panels may achieve an improved payback period and return on investment. The economic benefits are, however, highly sensitive to the energy market price fluctuations and the government incentives available for renewable energy (Feed in Tariffs, Green Certificates).

The PVT panels have been first introduced in the 1970s' (Kern and Russell, 1978) and have been slowly developing ever since, with increased research interest in the last decade. However, the PVT technology is not yet well-established in neither academic research field or on the commercial market. In recent years, the research on PVTs is focused on technology development, modeling, HVAC integration, and optimization. On one hand, research can focus on the development of PVT collectors in order to improve the design solutions and to increase the efficiency of solar energy conversion (Papoutsis et al., 2017; Bombarda et al., 2016; Guo and Zheng, 2017). On the other hand, the research can investigate the integration of PVT technologies in buildings to assess the operative performances and actual energy-economy benefits (Chow et al., 2005; Prabhakant and Tiwari, 2010; Agrawal and Tiwari, 2010). This study falls in the first category, aiming to develop an explicit PVT model that can assess the suitability of various design parameters in any ambient conditions, which can consequently lead to improving performance of the panel.

Various configurations of PVT have been developed, and their performance varies according to multiple parameters: optical, geometrical and thermo-physical properties, type of fluid, wind speed and direction, solar radiation and ambient temperature. A number of models have been identified in the literature for various configurations and climatic conditions. Rejeb et al. (2015) develops a sheet-and-tube PVT model and simulates its performance in Monastir, Tunisia. Aste et al. (2015) proposes a model to evaluate the daily and annual yield of a thin film roll-bond PVT collector in Milan, Italy. Chow et al. (2005) develops a seven-node model and simulates a sheet and tube panel.

A study by Brottier (2019) follows 28 PVT panels installations in France, Portugal and Switzerland. The instantaneous response of a PVT collector to various climatic conditions is analyzed in a paper by Armstrong and Hurley (2010). Some parametric studies have been carried out for establishing the influence of mass flow rate (Chow et al., 2005), thickness of insulation, wind speed and tube spacing (Rejeb et al., 2015). A box-channel model was developed and the influence of the channel dimensions was assessed in a study by Han et al. (2006). Most of these models are based on the same theoretical background, starting from the classical numerical model developed by Florschuetz (1979), based on the Hottel–Whillier–Bliss equations with various improvements, and the methodology of calculating the temperatures in the PVT layers is based on the exchange of energy between the layers and with the exterior.

A novel approach to simulating the operation of PVT panels is by using machine learning methods of artificial neural networks, least squares support vector machines and neuro-fuzzy. By comparing the performance of the three methods it was found that the least squares support vector machines method performed better than the other two, and is quite suitable for cases when experimental measurements are difficult or costly (Ahmadi et al., 2020; Zamen et al., 2019).

Another parametric study on a solar cooling system was done for the weather conditions of Athens, Greece (Tzinnis et al., 2016), and after optimization it achieved a solar coverage ratio up to 89.85%. An interesting research (Nhut et al., 2020) performed a parametric study of a solar-assisted house heating system coupled with a seasonal underground thermal energy storage tank, evaluating the annual energy production as a function of some of the main system parameters, such as the insulation thickness of the tank and the size of the tank.

Another parametric study was carried out on a grid-connected PV-battery systems investigating the effects of the weather, price of electricity, feed-in tariff, system cost, and electrical specifications from a technical–economical point of view (Khalilpour and Vassallo, 2016). Another study (Arsalis and Alexandrou, 2015) investigates a solar-heating-and-cooling system for a single-family household in terms of cost savings.

This paper proposes an explicit dynamic numerical model of a particular configuration of PVT panel (water-based roll-bond collector with Mono-Crystalline Silicon PV cells). The thermal model is able to evaluate the temperatures at each layer inside the collector, taking into account all the heat transfer processes between the layers or with the environment. Based on the output temperatures, the system performance indicators can then be assessed for various operational and constructive parameters. As a case study, the model is applied to the climatic conditions of Bucharest, Romania and Strasbourg, France. The novelty of this paper stands in the easy to follow and replicate methodology for simulating the operation of the panels, along with the comparison of its performance in two climatic conditions. The one-factor-at-a-time (OFAT) analysis carried out based on the numerical model reveals some useful design information for improving the performance of the collectors. Other aforementioned parametric studies have been carried out previously (Chow et al., 2005; Aste et al., 2015; Han et al., 2006), but the novelty of this research stands in the application of the model in various climatic conditions, besides from the OFAT analysis, and the analysis of not only the electrical and thermal performance, but also of the global and primary energy saving (PES) efficiencies.

2. Description of PVT collector

The PVT collector can take various configurations: liquid, air or dual liquid–air based, flat or concentrated. The thermal collector can also have multiple geometries (harp, direct flow, fractal) and manufacturing methods (sheet and tube, roll bond, rectangular channels). A typical PVT system is obtained by coupling a solar thermal collector at the back of a PV panel. A comprehensive review is carried out by Aste et al. (2014), which summarizes the various geometrical configurations, thermo-physical properties and manufacturing solutions for PVT systems. One of the most common configurations, which was also used in this study, is described below.

The PVT chosen panel is liquid based, with a direct flow geometry of the collector and roll bond channels (Fig. 1). The liquid-based exchanger was chosen due to its better heat transfer capacity compared to the air-based systems, in spite of its higher level of complexity. In addition, the liquid systems can be utilized directly for preheating domestic hot water (DHW). The direct flow channel was chosen for their simplicity and well proved experimental performance. The roll bond fabrication method is easy to achieve, very flexible in terms of geometry and relatively cheap to produce (Aste et al., 2014). The PV cell is Mono Crystalline

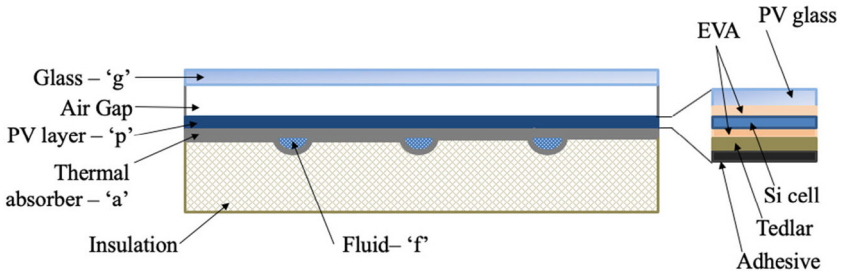

Fig. 1. Cross section of the PVT collector (Barbu et al., 2019a).

Silicon, with a reference electrical efficiency (η_{STC}) of 15% at the standard testing conditions (STC) - operating temperature (T_{ref}) of 25 °C, solar radiation of 1000 W/m^2 and wind speed 0 m/s. The temperature coefficient (β_T) is 0.5%/K. The relationship between the instantaneous electrical efficiency and the reference electrical efficiency is given below.

$$\eta_{EL} = \eta_{STC}[1 - \beta_T (T_c - T_{ref})] \quad (1)$$

where T_c is the temperature of the cell.

The collector fluid is a 30/70% glycol–water mix due to the fact that it provides better heat transfer parameters than plain water, and it has a lower freezing point, which is important in continental climates where winters are defined by negative temperatures. The size of the panel is 1 m x 2 m, and the diameter of the channel is 0.008 m, with a thickness of insulation of 5 cm. Table 1 summarizes the main PVT collector properties.

The cross section of the panel is shown in Fig. 1, with all the composing layers and the corresponding subscripts – glass (g), Air gap, PV layer (p), thermal absorber (a), insulation, fluid (f). The PV layer is made of PV glass, ethylene vinyl acetate (EVA) film, Silicon cell, Tedlar layer and adhesive.

The assumptions made for developing the model are:

- edges are well insulated; no heat is lost at the edges;
- the layers are very thin thus the vertical heat conduction can be assumed negligible;
- the optical properties of materials remain constant along the area;
- no dust effects or partial shading are taken into account;
- the flow rate of the fluid is constant, $\dot{m} = 0.05$ kg/s.
- the initial fluid inlet temperature at time $t = 0$ is $T_{i0} = 15$ °C. At every consecutive time step, the new T_{fi} is the average value between T_{i0}(assumed to be the cold-water inlet main temperature) and T_{fo} from the previous time step (the temperature of the fluid at the outlet of the panel).

The layers analyzed in this model are: glass, PV, thermal absorber and fluid. Some models (Chow et al., 2005; Pierrick et al., 2015) also analyze the behavior of the air gap layer and the insulation layer, but those temperatures were found not to be relevant for the purpose of this study, and thus the model is simplified to only compute the four layers of interest.

The thermal energy circulates through the layers of the PVT panel and to/from the exterior through three types of heat transfer processes: radiation, convection and conduction. Radiation is the process of heat transfer without any physical contact and it does not heat the transfer medium. Any physical body of a temperature greater than 0 K emits a level of radiation through electromagnetic waves. When radiation reaches a body, it can be either be absorbed, reflected or transmitted. Conduction is the movement of heat through a solid material or at the interface of two materials/layers that are in contact due to molecular collisions. Conduction that occurs on the solar panel is caused by the thermal gradients and its direction is from high temperature to low temperatures. Convection is the heat transfer in which energy moves within a fluid or gas through flow of matter from higher to lower temperature regions. It can be natural, occurring due to difference in densities, or forced by an external physical movement, such as a pump or the wind.

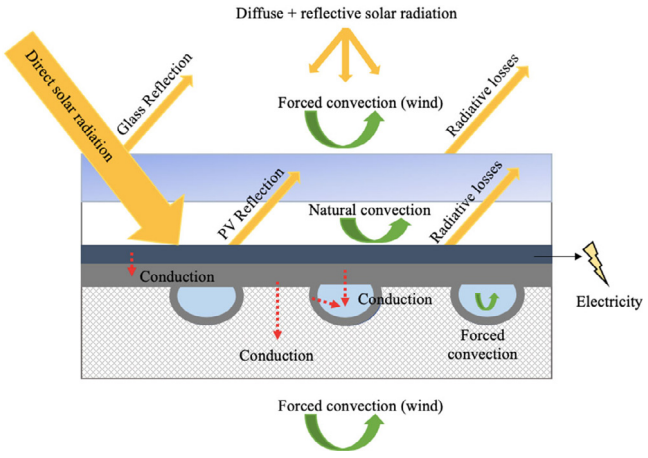

Fig. 2. Schematic heat transfer processes in the layer of a PVT panel.. (For interpretation of the references to color in this figure legend, the reader is referred to the web version of this article.)

The heat transfer processes that take place inside a PVT panel are shown in Fig. 2; radiation with a yellow arrow, convection in green and conduction in red. The glass layer receives direct and indirect solar radiation from the sun, a fraction of which is reflected, another part absorbed and the rest transmitted to the PV layer. It also receives reflected radiation and radiative losses from the PV layer. It loses some heat to the environment through forced convection caused by the wind. The PV layer receives a fraction of the solar radiation, of which some is reflected back to the glass layer and some is absorbed. The PV layer also loses heat through radiation to the glass. In addition, natural (free) convective heat transfer between the glass and the PV takes place inside the air gap. Out of the incident radiation, a fraction is converted to electricity through the photovoltaic effect. The absorber layer exchanges heat with the PV layer, with the insulation and with the fluid through conduction, and the insulation loses heat to the environment through forced convection from the wind. The heat transfer in the fluid occurs also through forced convection generated by the pumping system.

3. Implementation of numerical model

The numerical model was developed in a previous paper (Barbu et al., 2019b) and is presented in the next section.

Table 1
PVT properties (Rejeb et al., 2015; Aste et al., 2015; Pierrick et al., 2015).

Property	Glass	Air gap	PV	Thermal absorber	Fluid	Insulation	Unit
Emissivity (ε)	0.9	–	0.96	–	–	–	–
Absorbance (α)	0.1	–	0.9	–	–	–	–
Transmittance (τ)	0.93	–	–	–	–	–	–
Thickness (H)	0.004	0.02	0.006	0.001	–	0.04	m
Density (ρ)	2200	–	2330	2699	1050	16	kg/m^3
Specific heat (c)	670	–	900	800	[a]	1120	J/(kg K)
Thermal conductivity (k)	1.1	[a]	140	237	[a]	0.035	W/(m K)

[a]Depends on the temperature.

3.1. Heat balance

The numerical model is based on the heat transfer processes described in the previous section. A heat balance equation is developed for each of the significant layers of the system. This is based on the equation for the variation of internal energy in a physical body:

$$Mc\frac{dT}{dt} = \frac{dU}{dt} \tag{2}$$

where M [kg] is the mass, c [J/(kg K)] is the specific heat capacity, T [K] the temperature, dt [s] is the chosen time step and dU [J] is the change in internal energy of the layer.

3.2. Glass layer (g)

For the thermal balance of the **glass layer 'g'** we considered the convective and radiative losses from the glass to the environment ($Q_{g-e,CV}$ and $Q_{g-e,RD}$), the convective and radiative heat transfer from the glass to the PV layer ($Q_{g-p,CV}$ and $Q_{g-p,RD}$) and the heat absorbed by the glass (Q_g).

$$\begin{aligned} M_g c_g \frac{dT_g}{dt} &= Q_{g-e,CV} + Q_{g-e,RD} + Q_{g-p,CV} + Q_{g-p,RD} + Q_g \\ &= h_{g-e,CV}A_g\left(T_e - T_g\right) + h_{g-e,RD}A_g\left(T_{sky} - T_g\right) \\ &\quad + h_{gap}A_g\left(T_p - T_g\right) + h_{g-p,RD}A_g\left(T_p \right. \\ &\quad \left. - T_g\right) + A_g\alpha_g G_{irr} \end{aligned} \tag{3}$$

where $h_{g-e,CV}$ is the coefficient of forced convection between the glass and environment [W/(m^2 K)], A_g is the area of glass [m^2], T_e is the temperature of the environment [K], T_g is the temperature of the glass layer [K], $h_{g-e,RD}$ is the coefficient of radiative heat loss between the glass and environment [W/(m^2 K)], T_{sky} is the equivalent radiative temperature of the sky [K], h_{gap} is the thermal coefficient of the gap [W/(m^2 K)], T_p is the temperature pf the PV layer [K], $h_{g-p,RD}$ is the coefficient of radiative heat loss between the glass and the PV layer [W/(m^2 K)], α_g is the absorbance of the glass [–] and G_{irr} is the incident irradiation on the absorber [W/m^2].

Multiple reviews were carried out on the coefficient of forced convection due to wind ($h_{g-e,CV}$) (Rejeb et al., 2015; Aste et al., 2014), which can be expressed through various empirical correlations. The correlation proposed by McAdams (1954) was chosen for this study. It applies to winds speeds (v_w) from 0 to 10 m/s, gives good agreement between experimental and simulation data, and has been widely used in the literature for numerical PVT models (Rejeb et al., 2015; Lämmle, 2018).

$$h_{g-e,CV} = \begin{cases} 5.7 + 3.8v_w & for\ v_w < 5\ \dfrac{\mathrm{m}}{\mathrm{s}} \\ 6.47 + v_w^{0.78} & for\ v_w \geq 5\ \dfrac{\mathrm{m}}{\mathrm{s}} \end{cases} \tag{4}$$

The coefficient of radiative heat loss ($h_{g-e,RD}$) is calculated by using Stefan–Boltzmann constant ($\sigma = 5.67\times10^{-8}$ W m^{-2} K^{-4}), the emissivity of glass (ε_g) and the equivalent radiative temperature of the sky (T_{sky}). There are multiple equations available for defining the sky temperature, most commonly it can be expressed as a linear function of the ambient temperature (T_e) and the sky cloud coverage in octaves (N) (Aste et al., 2015). If clear sky conditions are assumed or there is no data available on the cloud coverage, Eq. (6) can be further simplified to Eq. (7), with less that 1% effect on the thermal and electrical output of the system (Guarracino et al., 2016; Touafek et al., 2014).

$$h_{g-e,RD} = \varepsilon_g\sigma({T_g}^2 + {T_{sky}}^2)(T_g + T_{sky}) \tag{5}$$

$$T_{sky} = 0.0552{T_e}^{1.5} + 2.652N \tag{6}$$

$$T_{sky} = 0.0552{T_e}^{1.5} \tag{7}$$

The thermal coefficient of the gap (h_{gap}) takes into account the conduction in the top layers of the PV sandwich (PV glass and EVA) and the convective heat transfer in the air gap.

$$\frac{1}{h_{gap}} = \frac{1}{h_{g-p,CV}} + \frac{H_{PVg}}{k_{PVg}} + \frac{H_{EVA}}{k_{EVA}} \tag{8}$$

$$h_{g-p,CV} = \frac{Nu_{air}k_{air}}{H_{gap}} \tag{9}$$

where H is the height of the layer (measured at the middle of the layer) [m], k is the thermal conductivity [W/(m K)] and Nu_{air} is the Nusselt number for air [–].

The Nusselt number correlation for inclined plates, tilt angles from 0 to 60, is given by Hollands et al. (1976). The radiative coefficient between the glass and the PV ($h_{g-p,RD}$) is expressed below:

$$h_{g-p,RD} = \frac{1}{\frac{1}{\varepsilon_g} + \frac{1}{\varepsilon_p} - 1}\sigma(T_g^2 + T_p^2)(T_g + T_p) \tag{10}$$

where ε_p is the emissivity of the PV layer [–] and ε_g is the emissivity of the glass [–].

3.3. PV layer (p)

The PV layer 'p' includes glass, two layers of EVA, cell and Tedlar. The thermal balance of the PV layer considers the convective and radiative heat transfer to the PV layer ($Q_{p-g,CV}$ and $Q_{p-g,RD}$), the conductive heat transfer to the absorber layer ($Q_{p-a,CD}$), the heat absorbed by the PV layer (Q_p) and electricity production (E).

$$\begin{aligned} M_p c_p \frac{dT_p}{dt} &= Q_{p-g,CV} + Q_{p-g,RD} + Q_{p-a,CD} + Q_p - E \\ &= h_{gap}A_p\left(T_g - T_p\right) + h_{p-g,RD}A_p\left(T_g - T_p\right) \\ &\quad + h_{p-a,CD}A_p\left(T_a - T_p\right) + A_p\left(\alpha\tau\right)_p G_{irr}(1 \\ &\quad - \eta_{EL(T)}) \end{aligned} \tag{11}$$

where A_p is the area of the PV layer [m^2], $h_{p-a,CD}$ is the conduction coefficient from the PV layer to the absorber [W/(m^2 K)], T_a is the temperature of the thermal absorber layer [K], and $\eta_{EL(T)}$ is the time dependent electrical efficiency of the cell [–].

The heat transfer coefficient in the air gap and the radiation coefficient are calculated in Eqs. (8)–(10). The conduction coefficient through the layers of EVA, Tedlar and adhesive is:

$$\frac{1}{h_{p-a,CD}} = \frac{H_{EVA}}{k_{EVA}} + \frac{H_{Ted}}{k_{Ted}} + \frac{H_{adh}}{k_{adh}} \tag{12}$$

The conversion efficiency of the cell decreases with the increase in the operating temperature T_p and depends on the temperature coefficient β_{PV}.

$$\eta_{EL(T)} = \eta_{STC}[1 - \beta_{PV}(T_p - T_{ref})] \tag{13}$$

where η_{STC} is the reference electrical efficiency measured at the standard operating temperature T_{ref} of 25 °C [–].

3.4. Thermal absorber (a)

The thermal balance of the **absorber layer 'a'** considers the conductive heat transfer to the PV layer ($Q_{a-p,CD}$), the heat transfer to the fluid (Q_{a-f}) and the heat loss to the exterior through the insulation ($Q_{a-e,CD}$).

$$M_a c_a \frac{dT_a}{dt} = Q_{a-p,CD} + Q_{a-f} + Q_{a-e,CD} = h_{a-p,CD}A_a\left(T_p - T_a\right) + h_{a-f}A_{ch}\left(T_f - T_a\right) + h_{a-e,CD}A_a\left(T_e - T_a\right) \tag{14}$$

where $h_{a-p,CD}$ is the heat transfer coefficient from the absorber to the PV layer [W/(m^2 K)], A_a is the area of the thermal absorber [m^2], A_{ch} is the area of the channel [m^2], h_{a-f} is the heat transfer coefficient of the fluid [W/(m^2 K)], T_f is the temperature of the fluid [K], $h_{a-e,CD}$ is the conductive heat loss coefficient to the environment [W/(m^2 K)].

The heat transfer coefficient to the PV layer ($h_{a-p,CD}$) is the same as in Eq (12). The heat transfer coefficient of the fluid depends on the type of flow (laminar or turbulent) (Incropera, 2011).

$$h_{a-f} = \begin{cases} 4.36\dfrac{k_f}{D_H}, & for\ Re < 2300\ [-] \\ 0.023\dfrac{k_f}{D_H}Re^{0.8}Pr^{0.4} & for\ Re \geq 2300\ [-] \\ 2\dfrac{k_f}{D_H}, & for\ \dot{m} = 0\ \dfrac{kg}{s} \end{cases} \tag{15}$$

where k_f is the thermal conductivity of the fluid [W/(m K)], D_H is the hydraulic diameter [m], Re is the Reynolds number [–], Pr is the Prandtl number [–] and $\dot{m}$ is the mass flow rate [kg/s].

3.5. Fluid (f)

The energy balance equation for the **fluid 'f'** considers the thermal energy coming from the absorber (Q_{f-a}) and the heat accumulated by the fluid (Q_f).

$$M_f c_f \frac{dT_f}{dt} = Q_{f-a} + Q_f = h_{a-f}\frac{\pi DL}{2}\left(T_a - T_f\right) + \dot{m}c_f\left(T_{fi} - T_{fo}\right) \tag{16}$$

The heat transfer coefficient of the fluid is calculated in Eq. (15), D is the diameter of the pipe and L the length [m], $\dot{m}$ [kg/s] is the mass flow rate of the fluid in the channels and the inlet and outlet temperatures are represented by T_{fi} and T_{fo} respectively [K].

$$T_f = 0.5T_{fi} + 0.5T_{fo} \tag{17}$$

3.6. System performance

The energy performance of the system can be computed in terms of thermal, electrical and overall efficiencies (η_{TH}, η_{EL}, $\eta_{overall}$). The electrical efficiency is calculated as the ratio between the power generated by the system (P_{EL}) and the amount of solar radiation incident on the surface of the collector (AxG $_{irr}$):

$$\eta_{EL} = \frac{P_{EL}}{AG_{irr}} \tag{18}$$

The standard equation for thermal efficiency is represented by the ratio between the amount of thermal energy generated by the system (Q_{TH}) and the solar radiation incident on the surface of the collector (AxG $_{irr}$):

$$\eta_{TH} = \frac{Q_{TH}}{AG_{irr}} = \frac{\dot{m}c_f(T_{fo} - T_{fi})}{AG_{irr}} \tag{19}$$

where $\dot{m}$ is the mass flow rate of the fluid and c_f is the specific heat capacity.

Another definition for the thermal efficiency was proposed by Bombarda et al. (2016), where distinction is made between the electrical and thermal power of the system, and thus the electrical power production is subtracted from the total incident irradiation. This definition allows for a more accurate comparison between the thermal performance of a PVT and stand-alone solar thermal system.

$$\eta_{TH}{}^* = \frac{Q_{TH}}{AG_{irr} - P_{EL}} = \frac{\dot{m}c_f(T_{fo} - T_{fi})}{AG_{irr} - P_{EL}} = \frac{\eta_{TH}}{1 - \eta_{EL}} \tag{20}$$

From the point of view of the first law of thermodynamics, the global efficiency of the system (η_{GL}) can be calculated as the sum of the thermal and electrical efficiencies. This is also known as the first law efficiency:

$$\eta_{GL} = \eta_{EL} + \eta_{TH} \tag{21}$$

Another approach is to consider the difference in grade between the two types of energy, i.e. electrical energy is a higher form of energy compared to the thermal. Thus, due to the fact that a kW_{el} cannot be directly compared to a kW_{th}, some authors (Aste et al., 2015; Huang et al., 2001) propose the primary energy saving efficiency (η_{PES}) as a more accurate way of assessing the system performance:

$$\eta_{PES} = \eta_{TH} + \frac{\eta_{EL}}{\eta_{Tpower}} \tag{22}$$

where η_{Tpower} is the average efficiency of producing electrical power, and it depends on the country of reference. On average, it can be assumed to be 0.4 (Aste et al., 2015), and this value was used for the calculations. For Romania, the average efficiency of producing electrical power in 2016 was 0.532, while in France it was 0.601 (European Environment Agency, 2018).

3.7. MatLAB implementation

By rearranging the energy balance equations (3), (11), (14) and (16), a system of coupled equations is obtained. The system of equations is then solved in MatLAB with the ordinary 'fsolve' function. The coefficients C and D are defined by rearranging the free terms of the energy balance equations above.

$$\begin{cases} C_1T_g + C_2T_p - D_1 = 0 \\ C_3T_g + C_4T_p + C_5T_a - D_2 = 0 \\ C_6T_p + C_7T_a + C_8T_f - D_3 = 0 \\ C_9T_a + C_{10}T_f - D_1 = 0 \end{cases} \tag{23}$$

where

$$C_1 = \frac{M_g c_g}{dt} + h_{g-e,CV}A_g + h_{g-e,RD}A_g + h_{gap}A_g + h_{g-p,RD}A_g \tag{24}$$

Table 2
Parameters of validation model (Bhattarai et al., 2012).

Collector size	2 m^2	Tube diameter	9 mm
Cell efficiency	17.3%	Mass flow rate	0.002 kg/m^2 s
Packing factor	80%	Solar radiation	1000 W/m^2
Temperature coefficient	−0.405%/K	Wind speed	1 m/s
No. of tubes	10	Ambient temperature	30 °C
Tube spacing	10 cm	Tilt angle	30°

$$C_2 = -h_{gap}A_g - h_{g-p,RD}A_g \tag{25}$$

$$D_1 = \frac{M_g c_g}{dt}T_g + h_{g-e,CV}A_g T_e + h_{g-e,RD}A_g T_{sky} + A_g \alpha_g G_{irr} \tag{26}$$

$$C_3 = -h_{gap}A_p - h_{p-g,RD}A_p \tag{27}$$

$$C_4 = \frac{M_p c_p}{dt} + h_{gap}A_p + h_{p-g,RD}A_p \tag{28}$$

$$C_5 = -h_{p-a,CD}A_p \tag{29}$$

$$D_2 = \frac{M_p c_p}{dt}T_p + A_p\,(\alpha\tau)_p\,G_{irr}(1-\eta_{EL(T)}) \tag{30}$$

$$C_6 = -h_{a-p,CD}A_a \tag{31}$$

$$C_7 = \frac{M_a c_a}{dt} + h_{a-p,CD}A_a + h_{a-f}A_{ch} + h_{a-e,CD}A_a \tag{32}$$

$$C_8 = -h_{a-f}A_{ch} \tag{33}$$

$$D_3 = \frac{M_a c_a}{dt}T_a + h_{a-e,CD}A_a T_e \tag{34}$$

$$C_9 = -h_{a-f}\frac{\pi DL}{2} \tag{35}$$

$$C_{10} = \frac{M_f c_f}{dt} + h_{a-f}\frac{\pi DL}{2} + 2\dot{m}c_f \tag{36}$$

$$D_4 = \frac{M_f c_f}{dt}T_f + 2\dot{m}c_f T_{fi} \tag{37}$$

The fsolve function solves the equations for each individual timestep and gives a vector solution for $[T_p\ T_g\ T_a\ T_f]$. The results are plotted on a graph and shown in Section 4. For the parametric study, a 'for' function is introduced to vary the variables in a chosen range, while keeping the rest constant.

3.8. Model validation

The developed model was validated by comparing the performance results to experimental data found in the literature. In order to achieve this, the PVT model described by McAdams (1954) is recreated using this model, with the same configuration and operating conditions used in the experiment. The variation of the thermal and electrical efficiency is plotted against the reduced temperature for both the simulated and experimental model. The characteristics of the experimental model are summarized in Table 2.

The system performance can be assessed by computing the electrical and thermal efficiencies, according to Eqs. (18)–(19). These are plotted against the reduced temperature, defined in Eq. (38) below, to account for the fact that the thermal efficiency is, in fact, dependent on ambient temperature, inlet temperature and global irradiation.

$$T^* = \frac{T_{fi} - T_{amb}}{G_{irr}} \tag{38}$$

Fig. 3 shows a good resemblance between the reference experimental data and the results obtained by the numerical model developed in this paper. It shows that under different operation conditions and constructive parameters of the collectors, the result of the experimental study from the literature can be recreated with the present numerical model.

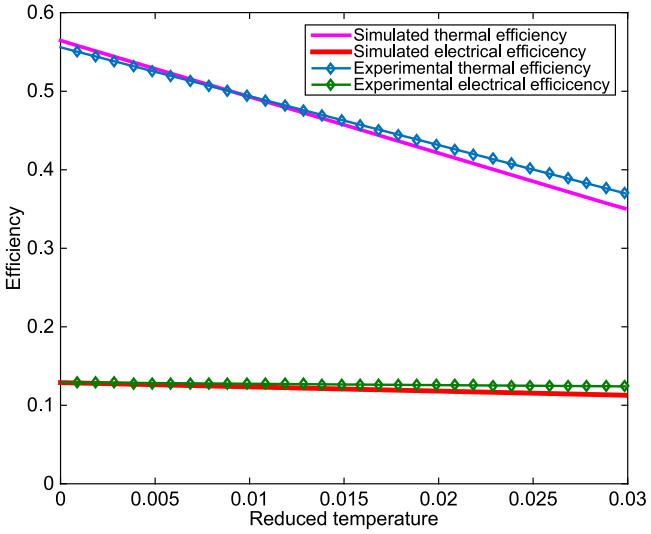

Fig. 3. Comparison of simulation and experimental results of thermal and electrical efficiencies as a function of the reduced temperature.

4. Results and discussion

4.1. Case studies

The developed numerical model was applied for a PVT panel in two different climate conditions: Bucharest and Strasbourg, which enables a comparison of the performance of the PVT system in both regions. The climate of Romania is temperate continental, with hot and sunny summers with occasional showers and thunderstorms and cold, cloudy winters and frequent snow and fog. In the southern region, where Bucharest is located, the winters are milder and the summers hotter. France's climate is temperate, with four specific regions. Alsace, where Strasbourg is located, is characterized by a continental climate which harbors cold winters, hot summers, and strong winds. The average summer months temperature in Bucharest is 29.1 °C, while in Strasburg it is 24.2 °C. For the winter months, Bucharest has an average of 4 °C, and Strasbourg 5.2 °C. The monthly summer sun hours are 278.8 and 222.0 for Bucharest and Strasbourg respectively, while the winter sun hours are 72.6 and 54.5 (WMO, 2019).

The variation of the weather during the day was used as an input into the numerical model in order to assess in real time the temperatures inside the panel. The input is: solar irradiation (G [W/m^2]), ambient temperature (Tamb [°C]) and wind speed (W [m/s]). The yearly profile with hourly resolution for each parameter was obtained from Meteonorm Database for both Bucharest, Romania and Strasbourg, France. The meteorological conditions of a typical day are presented in the figures below. Fig. 4a and b show the daily weather conditions for Strasbourg and Bucharest respectively from 8:00 to 20:00, with an hourly time resolution, while Fig. 5a and b show the winter weather conditions. Given the fact that the simulations were run for one day, it is important to note the sensitivity of the chosen data on the results of the numerical simulations. This means that the specific day which was chosen from the Meteonorm yearly database is of crucial importance and given the significant day to day variation of the weather, a random day can be misrepresenting the seasonal climate. In this case, the same data was chosen for both cities, making sure no extreme condition occur and the two weather conditions are comparable at the given time. The representative winter day is 3rd of January and for the summer is 12th of July.

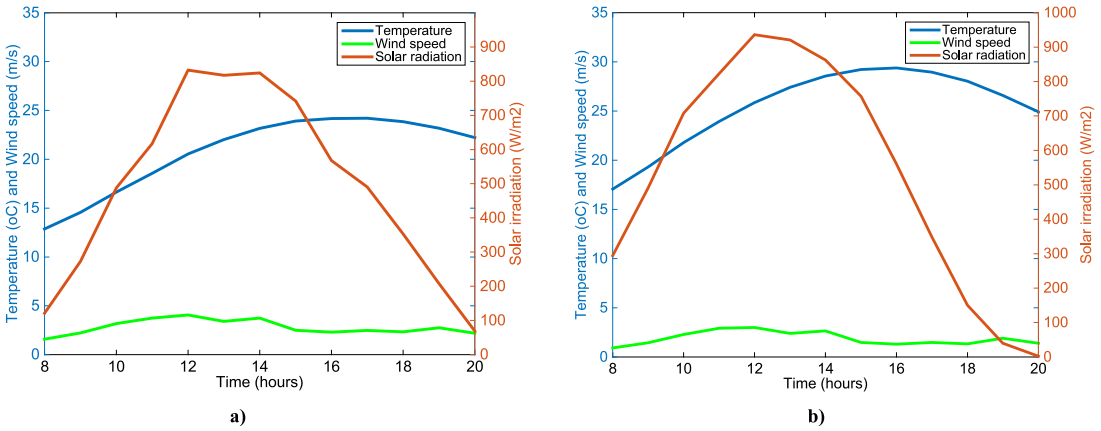

Fig. 4. Temperature, wind speed and solar radiation for a summer day in (a) Strasbourg (b) Bucharest.

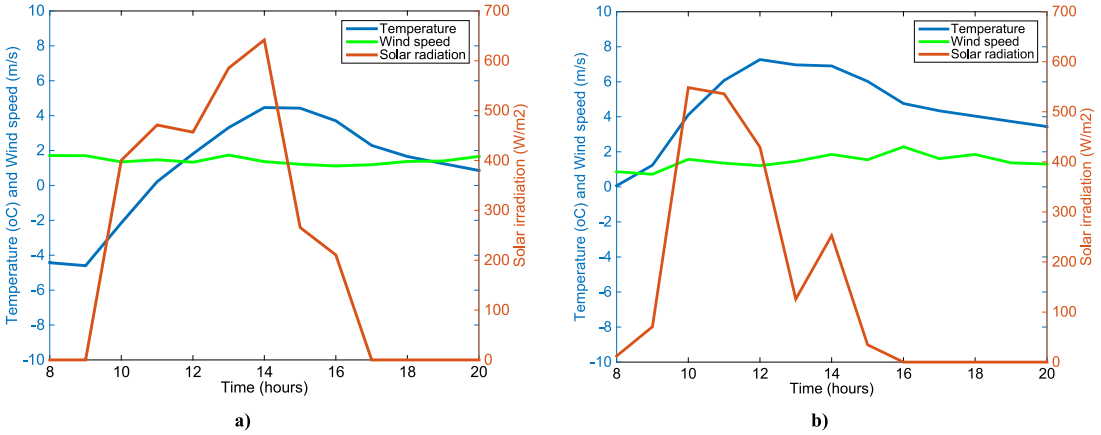

Fig. 5. Temperature, wind speed and solar radiation for a winter day in (a) Strasbourg (b) Bucharest.

Daily simulations were carried out for a typical summer and winter day in Bucharest, Romania and Strasbourg, France, from 8:00 to 20:00, with the weather data including ambient temperature, wind speed and irradiation, discussed in the previous section. Given these conditions, the time dependent temperature variation of the layers in the panel is shown below. Fig. 6a and b show the temperature evolution of the layers, as well as the ambient temperature, during a summer day in Strasbourg and Bucharest respectively. Fig. 7a and b show the temperature evolution of the layers, as well as the ambient temperature, during a winter day in Strasbourg and Bucharest respectively. As expected, the layers with the higher thermal conductivity reach the highest temperatures. In all cases, the PV layer is the most heated, reaching 52 °C for a summer day in Bucharest. The next layer is the thermal absorber, followed by the fluid. The glass layer is always the coolest. The temperature profile of all the layers follows closely the profile of the ambient temperature and global irradiation. The effect of the wind speed is not easily noticeable in the simulations. It can also be observed that the working fluid reaches slightly higher temperatures in Bucharest during the summer and in Strasbourg during the winter, due to their specific weather conditions. As a result, assuming that the system would have a water storage tank, it can be expected that the system would have a better thermal efficiency in Bucharest compared to Strasbourg during the summer, and higher in Strasbourg during the winter.

Table 3
Range of variation of parameters for OFAT parametric analysis.

Wind speed	0–10 m/s
Packing factor	75%–95%
Thickness of insulation	1–10 cm
Width (thickness) of tube	5–10 mm

4.2. Parametric analysis

Next, a OFAT analysis was carried out for some of the main constructive parameters of the panel, in order to evaluate their impact on the system efficiency. This is achieved by varying the parameters according to Table 3, while keeping the rest of them to the default values reported in Table 1. The reference electrical efficiency of the panel is 15%, while the thermal efficiency is dependent on ambient temperature, inlet temperature and global irradiation.

The effect of the two main meteorological conditions, ambient temperature and solar radiation, on the PVT behavior are easily observable in the case studies above. However, the influence of the third component, wind speed, is not so obvious, therefore this relationship is further analyzed by varying its value from 0 to 10 m/s and assessing the system performance. Increasing the wind speed results in a higher forced convection coefficient, according to Eq. (4). The results in Fig. 8 indicate a 2% decrease in the thermal efficiency, which can be explained by an increased forced convection heat loss from the glass to the ambient. On the other hand, a 0.1% increase in the electrical efficiency can be observed. A higher forced convection leads to a better cooling of the PV

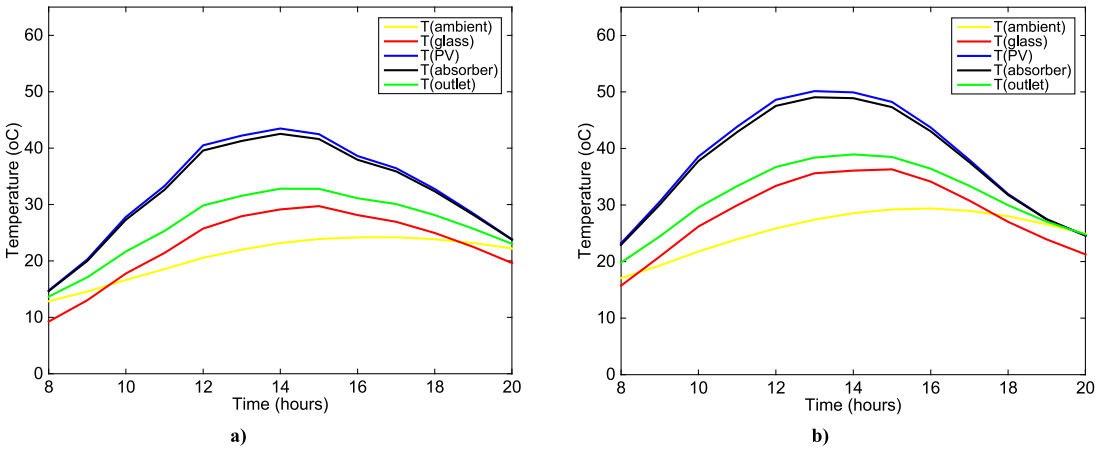

Fig. 6. Time dependent temperature evolution of PVT layers for a summer day in (a) Strasbourg (b) Bucharest.

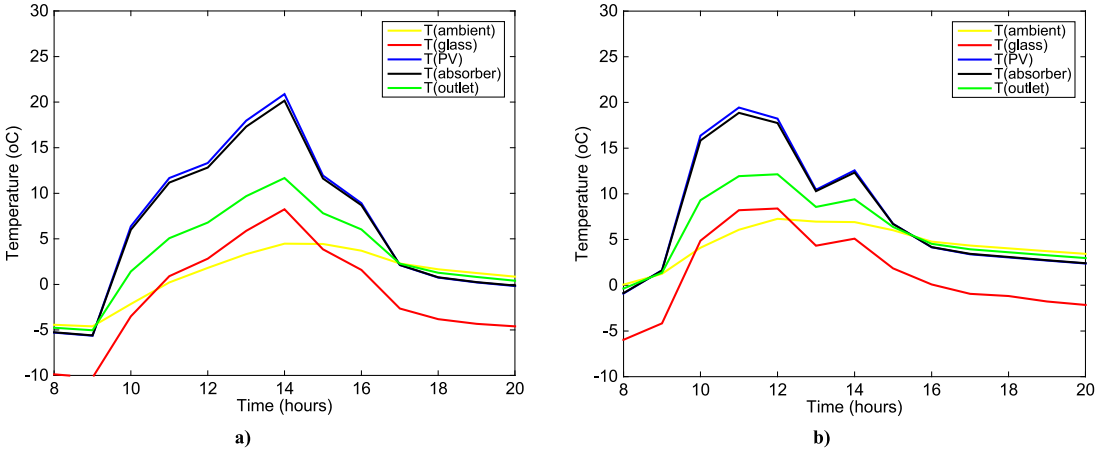

Fig. 7. Time dependent temperature evolution of PVT layers for a winter day in (a) Strasbourg (b) Bucharest.

cell and a lower operating temperature, which leads to a slightly improved electrical output. However, the effect of high wind speeds on the decrease in thermal performance is much more significant than the beneficial increase in electrical performance. Overall, the global efficiency decreases with higher wind speeds. It is also noticeable that the slope of electrical efficiency decreases gradually and tends towards flattening, which indicates that the operating temperature is close to reaching the STC value of 25 °C, after which cooling no longer has an effect on the electrical output.

Apart from the convective losses caused by the wind, heat losses also take place at the back of the panel through the layer of insulation, and their magnitude is directly influenced by the thickness of the layer. The effect of the insulation losses on the system performance can be assessed by a parametric variation of the insulation thickness, from 0.01 to 0.1 m. Fig. 9 shows a steep effect on both efficiencies at first, followed by a flattened curve, which indicates the fact that after a certain thickness, the increase in insulation has an insignificant effect on the panel performance. In the case of the electrical performance, this occurs at 0.05 m of insulation, where the PV cells reach the STC temperature. For the thermal performance, the curve is not completely flat even at 0.1%, but the slope decreases gradually. Again, as in the case of wind speed, the effect on the thermal performance is much more significant than on the electrical one, with a variation of 3.5% compared to 0.1%. Overall, the global efficiency increases with thicker insulation.

The effect of the packing factor of the PV cell on the system efficiency is illustrated in Fig. 10. Typical commercial cells have packing factors of 75% up to 95% for the highest performing ones. It can be observed that the increased packing factor has a significant positive effect on the electrical performance, with more than 2% improvement, due to a larger surface area of the panel being covered with PV cells, and implicitly, a larger amount of incident solar radiation being converted to electricity. The 20% decrease in thermal efficiency with higher packing factors is explained by the fact that a higher fraction of the solar energy is converted to electricity, and thus a smaller fraction remains to be converted into heat. Thus, the variation of the two efficiencies appears equivalent; However, depending on the consumer profile, it might be beneficial to choose a high packing factor for the PVT design, as the electrical energy is more valuable both economically and exergetically than the thermal energy. A high packing factor typically involves increased costs of the PV cells, thus a cost–benefit analysis should be carried out for optimum design. Overall, the global efficiency increases with a higher packing factor.

Finally, the width of the absorber channels is varied from 5 to 10 mm for a constant flow rate of 0.05 kg/s. A wider diameter channel results in a larger cross section area and thus a slower flow rate of the fluid in the channels, but also a larger area of heat transfer between the absorber and the fluid. A better performance of both components is observed with the increase in channel diameter, shown in Fig. 11. The electrical efficiency increases by 0.6% due to better cooling of the PV, while the significant increase of 20% in the thermal efficiency is explained by a better heat transfer between the absorber and the fluid,

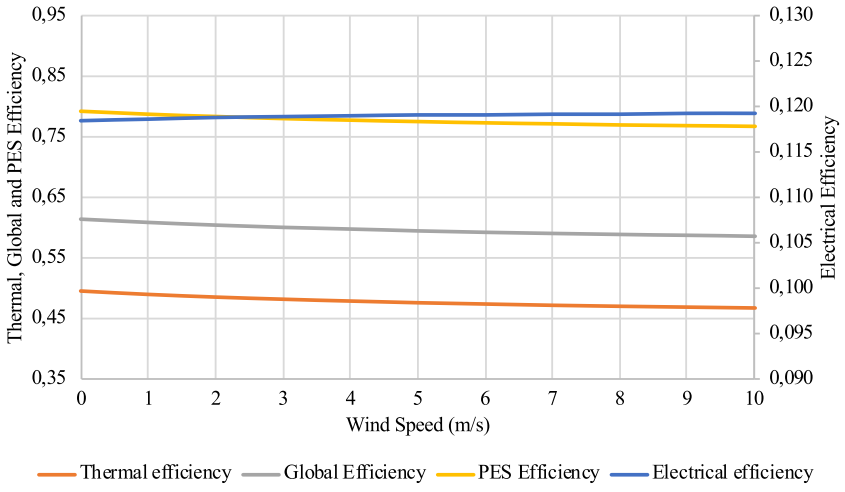

Fig. 8. Variation of thermal and electrical performance as a function of wind speed.

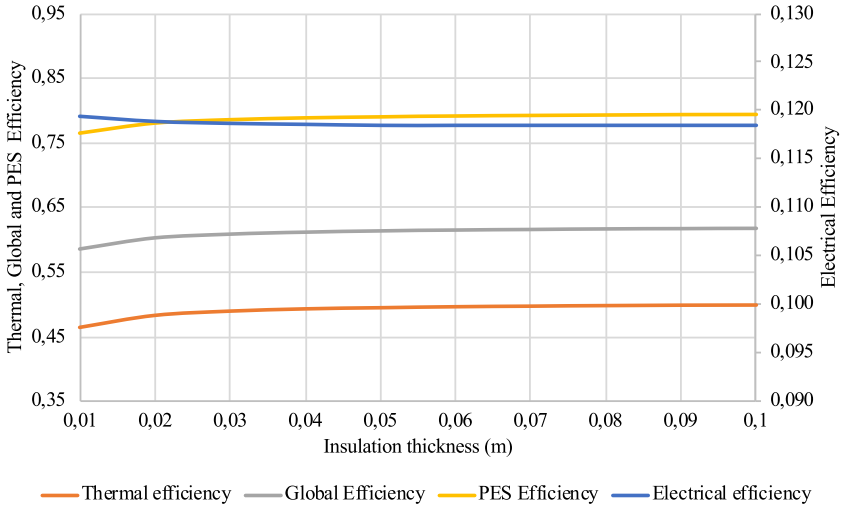

Fig. 9. Variation of thermal and electrical performance as a function of the thickness of insulation.

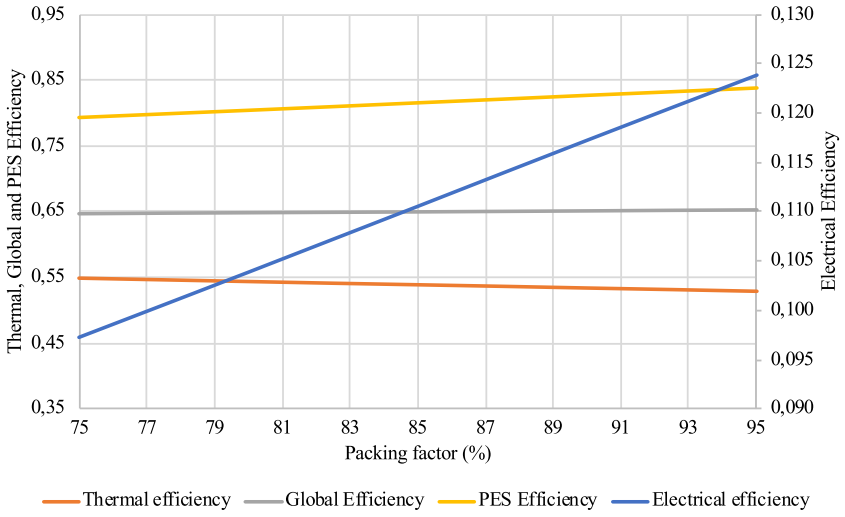

Fig. 10. Variation of thermal and electrical performance as a function of the packing factor.

and thus an improved thermal energy output. However, there are technical constrains on the fabrication methods of roll bond absorbers that limit the width to 8–10 mm depending on manufacturing method, materials and distance between the channels.

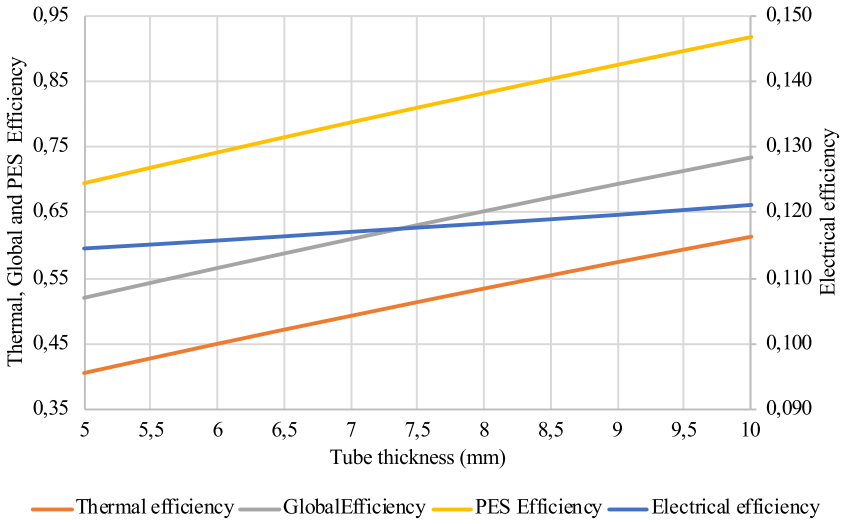

Fig. 11. Variation of thermal and electrical performance as a function of tube width.

Overall, the global and PES efficiencies increase with a higher tube thickness.

The results of the sensitivity analysis mostly indicate that, as in any cogeneration system, there is a compromise between the production of electrical and thermal power of the system. The design can lean towards improving one of the performances of the system. In most cases, the electrical performance will be more important, due to a higher value of electrical energy compared to thermal energy.

As a result of this analysis, a number of technical recommendations can be formulated for the efficient operation of PVT collectors. First of all, the roof installation of the panels is important, not only in terms of South-facing positioning (for the Northern hemisphere) and tilting it to a suitable angle according to the latitude of the location, but also in terms of wind protection. In some cases, space will be limited and there is no flexibility with the mounting, which can lead to high winds and a decrease in global efficiency of the collector. Where there is flexibility in the location, a rose wind is a useful tool for ensuring there is wind protection for the system of collectors, thus improving the overall efficiency. Wind protection is not only beneficial for the efficiency, but also decreases the amount of dust collected and reduces the maintenance costs. In terms of insulation, it was observed that the benefits of increasing its width are significant. However, this can add to the cost of production and can increase the bulkiness and weight of the equipment. Another technical solution is investigating alternative materials for the thermal insulation, with lower coefficient of thermal loss, so that both the thickness and thermal losses can be kept to a minimum. In terms of choosing a packing factor for the PV layer, it is important to keep in mind the end consumer and the applications. Some manufacturers have even started to produce two types of collectors, thermally driven and electrically driven, depending on the needs of the end user (ENDEF Solar Solutions, 2021). The width of the channels can be maximized but keeping in mind that there will be an increase in the pumping power for maintaining the required flow rate.

4.3. Performance maximization

The PVT panel can be optimized in order to maximize the production of either thermal or electrical energy, depending on the scope and building applications:

- electrical-driven – maximizing the electrical efficiency
- thermal-driven – maximizing the thermal efficiency
- compromise solution – maximizing the global efficiency

Table 4
Efficiency maximizing solutions.

	Electrical-driven solution	Thermal-driven solution	Compromise solution
Wind speed (m/s)	10	0	10
Insulation thickness (cm)	1	10	10
Packing factor (%)	95	75	95
Tube width (mm)	30	30	30

The results are summarized in Table 4. In the case of most parameters, the compromise solution coincides with the thermal-driven solution, except for the packing factor.

5. Conclusion and perspectives

This study proposed an explicit numerical model of a PVT collector based on the heat balance equations between each layer. The model has been validated by numerically recreating a panel that has been experimentally studied in the literature, and the results show good accordance. Next, the model was applied in two case studies for the climates of Bucharest, Romania, and Strasbourg, France. The input consists of ambient temperature, wind speed and global irradiance, which were obtained for both locations from the Meteonorm Database. Simulations were run for representative summer and winter days, from 8:00 to 20:00. The results show the temperature of each layer at any particular time, and it can be observed a slightly higher temperature of the working fluid in Bucharest during the summer, and in Strasbourg during the winter.

The OFAT parametric analyses carried out in this study showed in most cases a compromise between the electrical and thermal performance of the PVT system. In terms of wind speed and insulation, it was observed that the thermal benefits of low wind and high insulation overcome the decrease in electrical efficiency. For optimum design, the insulation thickness should be maximized and the wind speed minimized, which can be achieved by strategic placement of the panels in areas protected from wind. The packing factor was found to be optimum when maximized, as the electrical benefits are more significant than the thermal ones. The width of the channels in the heat exchanger should also be maximized as far as technologically possible for best performance.

Future work will be focused on setting up an experimental stand for a more direct validation of the model and of the analysis, and the dynamic coupling with residential consumers. Also, an algorithm for optimizing the design can be developed, taking into account the exergy of the system, the global performance, and the cost benefits.

Nomenclature

α	Absorbance [–]
α	Absorptivity [–]
A	Area [m^2]
ρ	Density [kg/m^3]
D	Diameter [m]
DHW	Domestic hot water
η	Efficiency [%]
E	Electrical energy [J]
$\dot{m}$	Flow rate [l/h]
Q	Heat [J]
h	Heat transfer coefficient [W/(m^2 K)]
HVAC	Heat, Ventilation, Air Conditioning
U	Internal energy [J]
L	Length [m]
M	Mass [kg]
Nu	Nusselt number [–]
OFAT	One factor at a time
PVT	Photovoltaic thermal
PV	Photovoltaic
P	Power [W]
Pr	Prandtl number [–]
PES	Primary energy saving
G	Radiation [W/m^2]
Re	Reynolds number [–]
N	Sky cloud coverage in octaves
ST	Solar thermal
c	Specific heat [J/(kg K)]
v	Speed [m/s]
STC	Standard test conditions
σ	Stefan–Boltzmann constant [W m^{-2} K^{-4}]
T	Temperature [°C]
β_T	Temperature coefficient [%/K]
t	Time [s]
H	Thickness [m]
k	Thermal conductivity [W/(m K)]
τ	Transmittance [–]
	Subscripts
adh	Adhesive
air	Air
c	Cell
CD	Conduction
CV	Convection
EL	Electrical
e	Environment
EVA	EVA
f	Fluid
gap	Gap
g	Glass
i	Inlet
irr	Irradiation
o	Outlet
p	PV layer
RD	Radiation
ref	Reference
sky	Sky
Ted	Tedlar
TH	Thermal
a	Thermal absorber

Declaration of competing interest

The authors declare that they have no known competing financial interests or personal relationships that could have appeared to influence the work reported in this paper.

References

Agrawal, B., Tiwari, G., 2010. Life cycle cost assessment of building integrated photovoltaic thermal (BIPVT) systems. Energ. Build. 42, 1472–1481.

Ahmadi, M.H., Baghban, A., Sadeghzadeh, M., Zamen, M., Mosavi, A., Shamshirband, S., Kumar, K., Mohammadi-Khanaposhtani, M., 2020. Evaluation of electrical efficiency of photovoltaic thermal solar collector. Eng. App. Comp. Fl. Mech. 14 (1), 545–565.

Ahmadi, M.H., Ghazvini, M., Sadeghzadeh, M., et al., 2018. Solar power technology for electricity generation: A critical review. Energy Sci. Eng. 6, 340–361.

Armstrong, S., Hurley, W.G., 2010. A thermal model for photovoltaic panels under varying atmospheric conditions. Appl. Therm. Eng. 30 (1488), 11–12–1495.

Arsalis, A., Alexandrou, A., 2015. Parametric study and cost analysis of a solar-heating-and-cooling system for detached single-family households in hot climates. Sol. Ene 117, 59–73.

Aste, N., Del Pero, C., Leonforte, F., 2014. Water flat plate PV-thermal collectors: A review. Sol. Energy 102, 98–115.

Aste, N., Leonforte, F., Del Pero, C., 2015. Design, modeling and performance monitoring of a photovoltaic-thermal (PVT) water collector. Sol. Energy 112, 85–99.

Barbu, M., Darie, G., Siroux, M., 2019a. Analysis of a residential photovoltaic-thermal (PVT) system in two similar climate conditions. Energies 12, 1–18. http://dx.doi.org/10.3390/en1219359.

Barbu, M., Mey-Cloutier, S., Siroux, M., Darie, G., 2019b. Dynamic modelling and sensibility analysis of a hybrid photovoltaic-thermal (PVT) system. In: 7th Eur. Conf. Ren. Energy Sys. 10, Madrid, Spain.

Barbu, M., Patrascu, R., Darie, G., Tutica, D., 2019c. A technical-economical analysis of the implementation of hybrid solar energy systems in small energy prosumer applications. Quality - Access Success 20 (169), 134–138.

Bhattarai, S., Oh, J.H., Euh, S.H., Krishna Kafle, G., Hyun Kim, D., 2012. Simulation and model validation of sheet and tube type photovoltaic thermal solar system and conventional solar collecting system in transient states. Sol. Energy Mater. Sol. Cells 103, 184–193.

Bombarda, P., Di Marcoberardino, G., Lucchini, A., Leva, S., Manzolini, G., Molinaroli, L., Pedranzini, F., Simonetti, R., 2016. Thermal and electric performances of roll-bond flat plate applied to conventional PV modules for heat recovery. Appl. Therm. Eng. 105, 304–313.

Brottier, L., 2019. Optimisation Biénergie D'un Panneau Solaire Multifonctionnel : Du Capteur Aux Installations in Situ ((PhD) Université Paris-Saclay). Paris.

Chow, T., Chan, A., Fong, K., et al., 2005. Energy performance of a solar hybrid collector system in a multistory apartment building. Proc. IMechE, Part A: J. Power Energy 219 (1), 1–11.

Dubey, S., Sarvaiya, J.N., Seshadri, B., 2013. Temperature dependent photovoltaic (PV) efficiency and its effect on PV production in the world – a review. Energy Procedia 33, 311–321.

ENDEF Solar Solutions, 2021. Hybrid solar collectors. [online] Available at: https://endef.com/en/hybrid-solar-panel/.

European Environment Agency, 2018. Efficiency of conventional thermal electricity and heat production in europe. Available online: https://www.eea.europa.eu/data-and-maps/indicators/efficiency-of-conventional-thermal-electricity-generation-4/assessment-2.

Florschuetz, L.W., 1979. Extension of the Hottel-Whillier model to the analysis of combined photovoltaic/thermal flat plate collectors. Sol. Energy 22, 361–366.

Guarracino, I., Mellor, A., Ekins-Daukes, N.J., Markides, C.N., 2016. Dynamic coupled thermal-and-electrical modelling of sheet-and-tube hybrid photovoltaic/thermal (PVT) collectors. Appl. Therm. Eng. 101, 778–795.

Guo, J., Zheng, L., 2017. Numerically study on a new hybrid photovoltaic thermal (PVT) collectors with natural circulation. Appl. Sol. Energy 53 (4), 316–321.

Han, J., Chow, T., Han, C., 2006. Effect of flow channel dimensions on the performance of a box-frame photovoltaic/thermal collector. Proc. IMechE, Part A: J. Power Energy 220 (7), 681–688.

Herrando, M., Markides, C., 2016. Hybrid PV and solar-thermal systems for domestic heat and power provision in the UK: Techno-economic considerations. Appl. Energy 161, 512–532.

Hollands, K.G.T., Unny, T.E., Raithby, G.D., Konicek, L., 1976. Free convective heat transfer across inclined air layers. J. Heat Transfer 98 (2), 189.

Huang, B., Lin, T., Hung, W., Sun, F., 2001. Performance evaluation of solar photovoltaic/thermal systems. Sol. Energy 70 (5), 443–448.
Incropera, F., 2011. Fundamentals of Heat and Mass Transfer. John Wiley and Sons.
Kern, E., Russell, M., 1978. Combined photovoltaic and thermal hybrid collector systems. In: IEEE Photovolt. Spec. Conf., Vol. 1. p. 1153.
Khalilpour, K., Vassallo, A., 2016. Technoeconomic parametric analysis of PV-battery systems. Ren. En. 97 75, 7–768.
Khatibi, A., Razi Astaraei, F., Ahmadi, M.H., 2019. Generation and combination of the solar cells: A current model review. Energy Sci. Eng. 00, 1–18.
Lämmle, M., 2018. Thermal Management of PVT Collectors - Development and Modelling of Highly Efficient Glazed, Flat Plate PVT Collectors with Low-E Coatings and Overheating Protection ((PhD) Fraunhofer Institute ISE).
McAdams, W.H., 1954. Heat Transmission, third ed. McGraw-Hill, New York.
Nhut, L., Raza, W., Park, Y., 2020. A parametric study of a solar-assisted house heating system with a seasonal underground thermal energy storage tank. Sustainability 12 (8686).
Papoutsis, E., Koronaki, I., Papaefthimiou, V., 2017. Numerical simulation and parametric study of different types of solar cooling systems under mediterranean climatic conditions. Energ. Build. 138, 601–611.
Pierrick, H., Christophe, M., Leon, G. others, 2015. Dynamic numerical model of a high efficiency PV-T collector integrated into a domestic hot water system. Sol Energy 111, 68–81.
Prabhakant, Agrawal B., Tiwari, G., 2010. Return on capital and earned carbon credit by hybrid solar Photovoltaic—wind turbine generators. Appl. Sol. Energy 46 (1), 33–45.
Ramos, A., Guarracino, I., Mellor, A., Alonso-Alvarez, D., Childs, P., Ekins-Daukes, N.J., Markides, C.N., 2017. Solar-Thermal and Hybrid Photovoltaic-Thermal Systems for Renewable Heating. Grantham Institute Briefing paper No 22, Imperial College London..
Rejeb, O., Dhaou, H., Jemni, A., 2015. Parameters effect analysis of a photovoltaic thermal collector: Case study for climatic conditions of monastir. Tunisia. Energy Convers. Manag. 89, 409–419.
Touafek, K., Khelifa, A., Adouane, M., 2014. Theoretical and experimental study of sheet and tubes hybrid PVT collector. Energy Convers. Manag. 80, 71–77.
Tzinnis, S., Bellos, E., Tzivanidis, C., 2016. Parametric analysis of a solar cooling system designed for athens climate. In: EinB2016–5th International Conference ENERGY in BUILDINGS 2016.
WMO, 2019. WMO - world meteorological organization. In: Country Profile Database.
Zamen, M., Baghban, A., Pourkiaei, S.M., Ahmadi, M.H., 2019. Optimization methods using artificial intelligence algorithms to estimate thermal efficiency of PV/T system. Energy Sci. Eng. 00, 1–14.